Journal of Materials Chemistry A

Accepted Manuscript

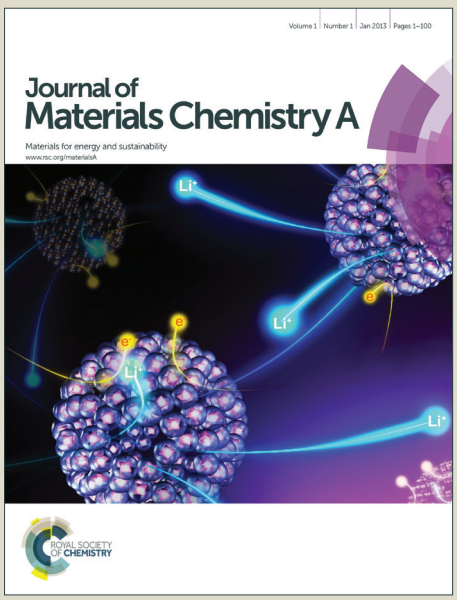

ROYAL SOCIETY OF CHEMISTRY

www.rsc.org/materialsA

Journal of
Materials Chemistry A

RSCPublishing

PAPER

Site-selected synthesis of novel Ag@AgCl nanoframes with efficient visible light induced photocatalytic activity

Cite this: J. Mater. Chem. A, 2014,

Received 00th March 2014,
Accepted 00th May 2014

DOI: 10.1039/x0xx00000x

www.rsc.org/MaterialsA

Changcun Han,[ab] Lei Ge,* [ab] Changfeng Chen,[b] Yujing Li,[b] Zhen Zhao,[a] Xinlai Xiao,[b] Zhiliang Li,[b] and Junlong Zhang[b]

A novel and facile synthetic route toward Ag@AgCl nanoframe photocatalysts is developed. The AgCl nanoframes were initially prepared via a site-selected growth process. After light irradiation, the Ag@AgCl composite nanoframes with uniform distribution of Ag nanoparticles on the surface were successfully synthesized. The physical and photophysical properties of the Ag@AgCl composite photocatalysts were characterized by X-ray diffraction (XRD), scanning electron microscopy (SEM), ultraviolet-visible diffuse reflection spectroscopy (DRS), X-ray photoelectron spectroscopy (XPS), electron spin resonance (ESR) and photoluminescence spectroscopy (PL). The Ag@AgCl nanoframes showed superior photocatalytic activity and photo-generated charge carrier separation efficiency under visible light irradiation, when compared with pure AgCl and Ag@AgCl cubic structures. Furthermore, the Ag@AgCl nanoframes can maintain photocatalytic activity after 5 cycles. A possible mechanism for Ag@AgCl nanoframe structures is proposed. The enhanced photocatalytic activity of Ag@AgCl nanoframe structures can be attributed to the surface plasmon resonance (SPR) effect from Ag and hybrid effect from AgCl.

1. Introduction

Semiconductor photocatalytic materials have attracted considerable attention due to their potential application in solving current issues such as energy conservation, environmental pollution and global warming.[1-6] Among various semiconductor materials, titanium dioxide (TiO_2) has been widely studied for its excellent photocatalytic properties, low cost, chemical stability and nontoxicity.[2,7-10] However, owing to the large band gap of TiO_2 (3.03 eV for rutile and 3.2 eV for anatase), its excitation requires light with wavelength in UV range, leading to low utilization efficiency of the solar spectrum.[11] Meanwhile, photo-generated electron-hole pairs can easily recombine before migrating to the active sites, which significantly limits its photocatalytic applications.[12] Many efforts have been focused on the exploration of efficient visible-light-induced photocatalysts to meet the requirements of future technologies based-on solar energy.[13-16]

Recently, the noble-metal nanoparticles (NPs), such as Au[17] and Ag, [18, 19] are found to strongly absorb visible light due to surface plasmon resonance (SPR) effect. As a consequence, plasmonic nanoparticles may serve as alternative sensitizers to enhance the absorption of wide band-gap photocatalysts in the UV-visible regions, and the resulting composite catalysts can maintain stability as well.[20] Recently, many studies have indicated that silver/silver compounds (Ag/AgX, X= Cl, Br, I, PO_4, CO_3, O, etc.) possess excellent photocatalytic activity due to the SPR effect of noble metal nanoparticles under light irradiation. [21-27] An et al.[28] synthesized cube like Ag@AgCl plasmonic photocatalyst by one-pot approach in ethylene glycol solvent with polyvinylpyrrolidone (PVP). The as-synthesized samples exhibit high efficiency for decomposition of methylene blue (MB) under sunlight illumination. Tang et al.[29] synthesized Ag@AgCl cubic cage photocatalysts by a novel sacrificial salt-crystal-template process, and directly observed plasmon-induced electron transfer from Ag nanoparticles to AgCl surface with ultrafast injection time spectra within 150 fs. Dong et al [30] prepared uniform cubic Ag@AgCl photocatalysts by a mild controllable double-jet precipitation technique, and confirmed that $\cdot O_2^-$ and Cl^0 are likely to be the reactive species leading to the degradation of organics. It has been proved that the photocatalytic activities were closely related to the structure of the photocatalysts. In particular, the nanoframe and nanocubic cage structures, with specific morphology and high order, have been concerned due to their important role in the systematic study of structure-performance relationship. Alternatively, if noble metal particles could be directly grown over a semiconductor substrate via a in-situ redox reaction, the catalytic activity of the resulting hybrid composite would be significantly enhanced.[31] In the present, designing a general route for rational synthesis of a series of nano-materials for emerging applications has become more and more fascinating,

which can provide a way to design new types of nano-materials with desired properties via a given methodology.[32]

Herein, we explore a general strategy to fabricate uniform AgCl nanoframes by templating against NaCl nanocrystals, and then obtain the Ag@AgCl composite nanoframes via simple photo-reduction of as-prepared AgCl samples. In particular, the key factors ($AgNO_3$ and NaCl solution volume ratio, Ag^+ ions concentration) that determine the morphology of Ag@AgCl nanoframes were investigated. The photocatalytic activity of Ag@AgCl plasmonic samples was investigated by degradation of the methyl orange (MO). Moreover, the photocatalytic mechanism was investigated by electron spin resonance (ESR) technique. The novel Ag@AgCl nanoframe structures may have potential applications in environmental purifications.

2. Experimental

2.1 Materials

Silver nitrate ($AgNO_3$, Sigma-Aldrich, 99%), sodium chloride (NaCl, 99.5% A.R.), polyvinylpyrrolidone (PVP, Sigma-Aldrich, K29-32, average Mw=58000), ethyl alcohol (EtOH, A.R.) and methyl orange (MO, AR) were used as received without additional purification or treatment. Milli-Q water was used as the solvent for all of the solutions or dispersions.

2.2 Synthesis of Ag@AgCl nanoframe structures

The Ag@AgCl nanoframes were firstly prepared through the reported method with slight modification.[29] First, the AgCl nanoframes were synthesized by sacrificial water soluble salt crystal template and sited-section replacing growth process. In a typical procedure, $AgNO_3$ ethanol solution was prepared by dissolving 170mg $AgNO_3$ and 1200mg polyvinylpyrrolidone K29-32 (PVP) in 20ml anhydrous ethanol. NaCl saturated aqueous solution was also prepared in advance. Then, NaCl saturated aqueous solution (3ml) was injected into 100ml anhydrous ethanol solution under constant stirring vigorously, and a white suspension was formed immediately. Subsequently, 20ml $AgNO_3$ ethanol solution was poured into the NaCl ethanol dispersion, the mixture was vigorously stirred for 24h, and the NaCl@AgCl core-shell nanoframes were obtained. The products were collected after centrifugation and washed 4-6 times with distilled water to remove the PVP and residual ions (Na^+ and Cl^-).

The synthesis process of Ag@AgCl nanoframes was described as follows: 0.2g AgCl nanoframes dispersed into 20ml ethanol solution. Then, Ag nanoparticles were obtained on the surface of AgCl by photo-reduction technique. In the photo-reduction process, the ethanol dispersion was illuminated using solar simulator 300W Xe lamp (PLS-SXE300, Beijing Perfect light Technology Co., Ltd) for 0, 30 and 60 min, the resulting samples were denoted as A-0, A-30 and A-60, respectively. All the samples were finally collected after centrifugation, washed with ethanol and deionized water, and dried in an oven at 60°C.

2.3 Characterization

The crystal structure of the sample was investigated using X-ray diffraction (XRD; Bruker D8 Advance, X-ray diffractometer) with CuKa radiation at a scan rate of $4min^{-1}$. The acceleration voltage and the applied current were 40kV and 40mA, respectively. The morphology of the samples was examined by field emission scanning electronic microscope (FESEM, FEI Quanta 200F; accelerating voltage=10kV). UV-Vis diffuse reflection spectroscopy (DRS) was performed on a Shimadzu UV-4100 spectrophotometer using $BaSO_4$ as the reference material. The X-ray photoelectron spectroscopy (XPS) was measured in a PHI 5300 ESCA system. The beam voltage was 3.0eV, and the energy of Ar ion beam was 1.0 keV. The binding energies were normalized to the signal for adventitious carbon at 284.6eV (Fig. 5D). The electron spin resonance (ESR) signals of spin-trapped oxidative radicals were obtained on a Bruker model ESR JES-FA200 spectrometer equipped with a quanta-Ray Nd:YAG laser system as the light source with a UV-cutoff filter ($\lambda \geq 400nm$). The PL spectra of the photocatalysts were detected using a Varian Cary Eclipse spectrometer with excitation wavelength of 395 nm.

2.4 Evaluation of photocatalytic performance

The photocatalytic activities of the as-prepared samples were evaluated by photo-degradation of the methyl orange (MO) dye in aqueous solution under visible-light irradiation. In a typical photocatalytic experiment, 0.05 g photocatalyst powder was suspended in 200 ml MO aqueous solution (10 mg L^{-1}). The solution was pre-stirred vigorously in the dark 60 min to establish adsorption-desorption equilibrium. After that, a solar simulator 300W Xe lamp (PLS-SXE300, Beijing Perfect light Technology Co., Ltd) coupled with a UV-cutoff filter (400nm) was used as the visible light source to irradiate the suspension under vigorous stirring. The light intensity employed was 72 $mW \cdot cm^{-2}$. Samples were collected from the reaction mixture every 5min, centrifuged to remove the photocatalysts, and analyzed quantitatively for the absorption peak at 505nm using UV-1700 spectrometer. Additionally, Ag@AgCl nanoframes after the above-mentioned first cycle experiment were centrifuged and collected for subsequent recycling tests. All procedures for the recycling test are the same as the first cycle.

3. Results and discussion

3.1 Characterization of Ag@AgCl nanoframe samples

The overall fabrication procedures of the plasmonic Ag@AgCl nanoframes are schematically illustrated in Fig.1. A sited-section process was used to synthesize Ag@AgCl samples with nanoframe morphology. Moreover, through controlling the structure and pecking of the building block nanocrystals, it also gives the possibility to construct desired nanocrystal superlattices and tailor their properties. NaCl crystal templates were prepared by injecting saturated NaCl aqueous solution into anhydrous ethanol. $AgNO_3$ (PVP) solution was subsequently added into the NaCl dispersion, along with the assistance of PVP to prevent the aggregation of AgCl nanoparticles. Ion exchange diffusion reaction between NaCl and Ag^+ in the solution led to the heterogenous nucleation and continued growth of AgCl on the arris of the NaCl template, as shown in Fig.1A. After AgCl nanoframes formed on NaCl crystal surface, the de-ionized water was used to dissolve NaCl crystal in Fig.1B process. In Fig.1C description, AgCl nanoframes were covered by the Ag nanoparticles, forming the stable Ag@AgCl nanoframes after light irradiation. Under UV-light irradiation, AgCl will produce an electron and a hole after absorbing a photon, and subsequently the electron combines with silver ion to form Ag^0 atom.

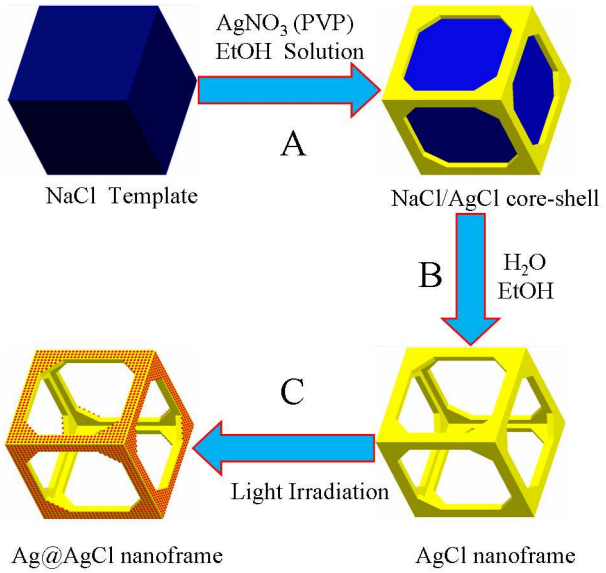

Fig.1 Schematic illustration of the formation route of Ag@AgCl nanoframe photocatalysts: A) The $AgNO_3$ solution with PVP was added into NaCl ethanol suspension; B) Dissolving NaCl by water; C) Light irradiation.

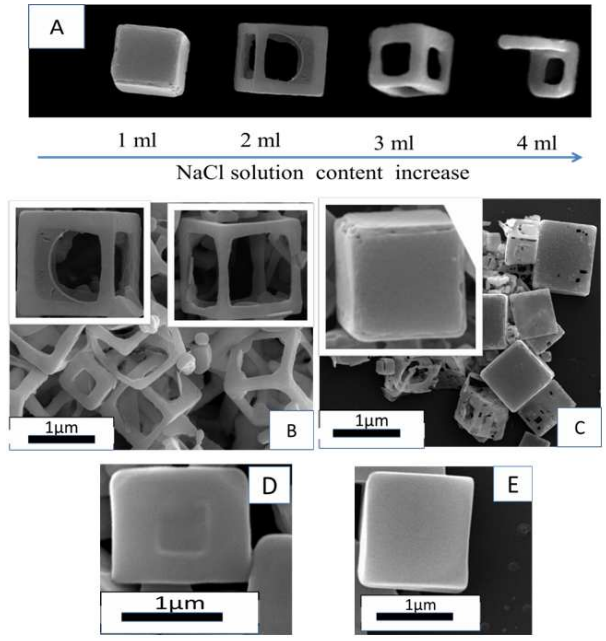

Fig. 2 (A) Schematic illustration of the morphological and structural changes; (B) SEM images of the obtained Ag@AgCl nanoframes; (C)Ag@AgCl cubic cages; (D) Ag@AgCl precursor materials, after washing and light reduction into the final product B; (E) Ag@AgCl cubic cages precursor materials, after washing and light reduction into the final product C. (inset: a mono-disperse SEM image of the product).

Fig. 2 presents typical scanning electron microscopy (SEM) images of the Ag@AgCl nanoframes. Fig.2 (A) shows the morphological and structural changes involved in the preparation of Ag@AgCl nanoframes with the increase of sodium chloride contents. The mono-dispersed Ag@AgCl nanoframes (ca.1.0-1.3um in edge length) were successfully prepared with clearly defined edges (Fig. 2B). The phenomenon results from the contribution of the high viscosity of the PVP solvent, which may significantly reduce the diffusion coefficients of both Ag^+ and Cl^-, and depress the nucleation and growth rate of the AgCl.

The X-ray diffraction (XRD) patterns of Ag, AgCl and Ag@AgCl nanoframes are showed in Fig.3. The Ag@AgCl samples (A-30) exhibit diffraction peaks at approximately 2θ=27.8°, 32.2°, 46.2°, 54.8° and 57.5°, which can be indexed to the AgCl (111), (200), (220), (311) and (222) planes, respectively (JCPDS No. 85-1355).[33] However, unlike AgCl, Ag@AgCl (A-30) shows a weak peak around the scattering angle of 2θ=38.2° (Fig.3, inset), which can be ascribed to the cubic phase of metallic Ag (JCPDS No. 65-2871).[34] This results indicates that photo-reduction is an efficient method for producing metallic Ag NPs on the surface of AgCl grains. No characteristic peaks attributing to impurities or other phases (such as Ag_2O) are detected, demonstrating that the obtained products are composed of AgCl and metallic Ag.

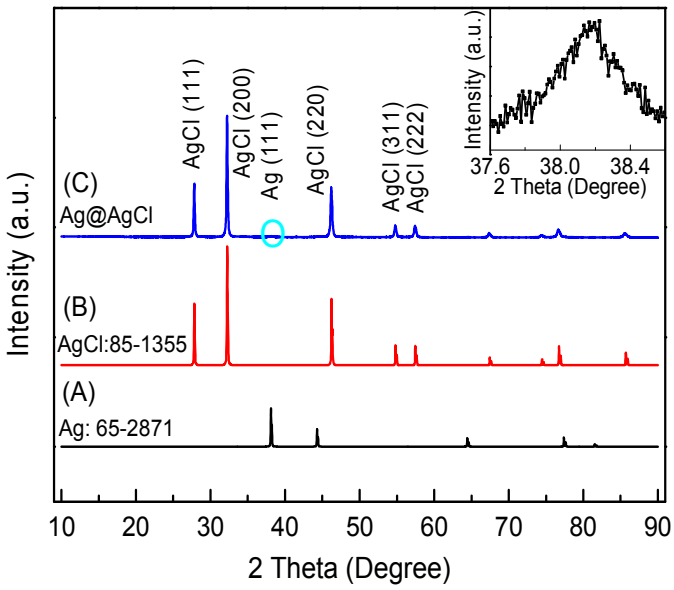

Fig. 3 XRD patterns of as-prepared samples: (A) Ag, (B) AgCl and (C) Ag@AgCl nanoframes (A-30).

The UV-Vis diffuse-reflectance spectra of AgCl and Ag@AgCl (A-30) are illustrated in Fig. 4. Compared to the pristine AgCl, the Ag@AgCl exhibits a stronger absorption in both the ultraviolet and visible light regions. This is attributed to the plasmon resonance of silver nanoparticles deposited on AgCl nanoframes. The absorption around 390nm could be attributed to the characteristic absorption of localized surface plasmon absorption of the Ag nanoparticles covering the surface of AgCl, which is in accordance with the previous literature.[35] Therefore, the incubation of Ag nanoparticles in light irradiation provides an efficient way to acquire strongly visible-light responsive Ag@AgCl photocatalysts. Based on the DRS spectra, the band-gap of the as-prepared A-30 sample was determined to be 3.03eV, which similar to the previous literature.[36]

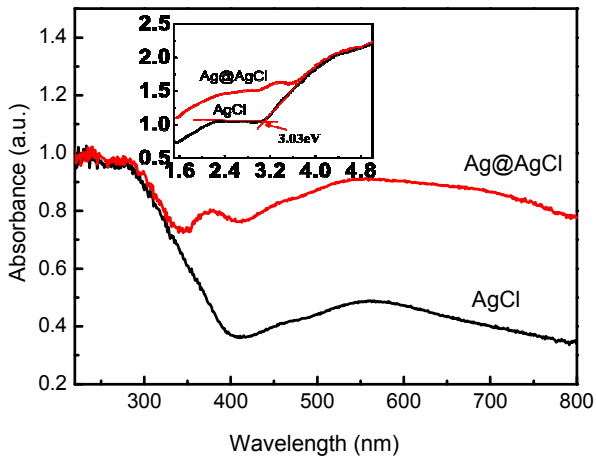

Fig. 4 UV-visible diffuse reflectance spectrum of the samples: (A) AgCl; (B) Ag@AgCl (A-30).

The elemental composition and chemical status were further investigated by XPS. Fig.5 (A-D) shows the XPS spectra of the as-prepared Ag@AgCl sample (A-30). Fig.5A displays the survey XPS spectrum of the as-prepared Ag@AgCl, which mainly contains the peaks of Ag, Cl and C. The carbon signal is due to the adventitious hydrocarbon from the XPS instrument itself. The sources of the Ag and Cl peaks correspond to the obtained samples. Fig.5B shows the Ag 3d XPS spectrum of sample A-30. The fitted Ag 3d peaks indicate that two components coexist in Ag $3d_{5/2}$ and Ag $3d_{3/2}$ signals, giving peaks at 367.2 and 368.2 eV for $3d_{5/2}$ as well as 373.2 and 374.0 eV for Ag $3d_{3/2}$. The peaks at 367.2 and 373.2 eV can be attributed to Ag^{+}, whereas the peaks at 368.2 and 374. 0 eV can be ascribed to Ag^{0}, according to previous reports.[23, 37, 38] The spectra of Cl 2p (Fig.5C) demonstrate that the binding energies of Cl $2p_{3/2}$ and Cl $2p_{1/2}$ are 197.6 and 199.2 eV. The XPS results confirm the existence of Ag^{0} in Ag@AgCl, consistent with the XRD results (Fig. 2).

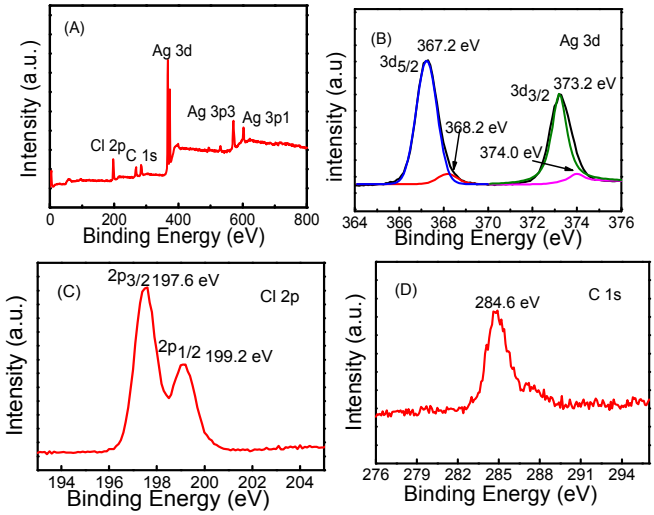

Fig.5 XPS spectra of the Ag@AgCl nanoframes (A-30): (A) the survey spectra (B) Ag3d (C) Cl 2p.

3.2 Photocatalytic performance of Ag@AgCl nanoframes

The photocatalytic activity of the obtained Ag@AgCl nanoframe was evaluated by the degradation of organic dyes under visible light irradiation. Methyl orange (MO) was chosen as a representative hazardous dye to evaluate the photocatalytic performance, which showed a major absorption band at 505nm. The photo-degradation process of MO was recorded by the temporal evolution of the spectrum and all of the samples were processed in the same procedure. The degradation curves of MO over Ag@AgCl photocatalyst as a function of irradiation time are plotted in Fig.6, at a certain time interval. The blank test confirms that methyl orange is only slightly degraded in the absence of photocatalysts, indicating that the photolysis can be ignored. For comparison, the photocatalystic activity of P25 was also examined in the same system under the same conditions. For A-0 sample, at the beginning of the visible light irradiation, there is only slight degradation. With increase of the illumination time, the photocatalytic activity is enhanced. However, with a further increase of illumination time (A-60), the catalytic activity is not significantly increased. Ag nanoparticles are gradually enriching at the surface of the AgCl in visible light irradiation, and which reaches steady state at 30 min (A-30 sample). Furthermore, the MO dye is almost completely decomposed after only 30min under visible light irradiation in the presence of the obtained Ag@AgCl photocatalyst. No absorbance peak is observed after irradiated for 30min, which indicates complete methyl orange decomposition. It is reasonable to ascribe the remarkable visible photocatalytic activity of Ag@AgCl to the SPR effects of Ag NPs.[22]

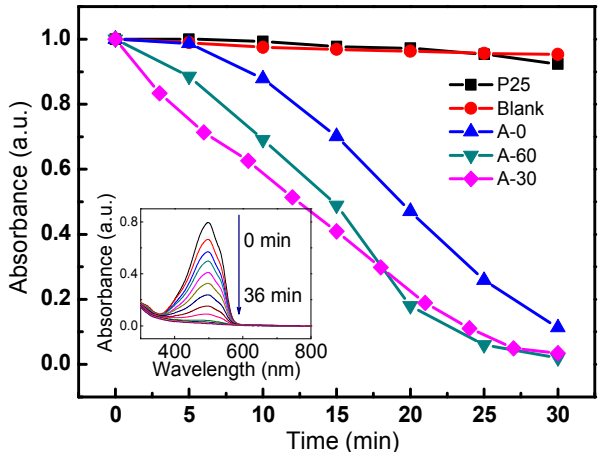

Fig. 6 The degradation curves of MO over Ag@AgCl nanoframe photocatalysts.

Due to the importance of the stability of a photocatalyst for its practical application, the photocatalytic stability of the obtained product was further investigated the cycling photo-degradation experiments. As shown in Fig.7, the photocatalytic performance of A-30 photocatalyst showed no obvious loss even after six cycle degradation of MO. However, only a slight inactivation was observed on A-30 sample after 8 photocatalytic cycles. Variations in the XRD analysis (Fig.8) also illustrated that the crystal structure of the Ag@AgCl photocatalyst did not change after the photocatalytic reaction. Therefore, the Ag@AgCl nanoframes can be regarded as stable photocatalysts under visible light irradiation.

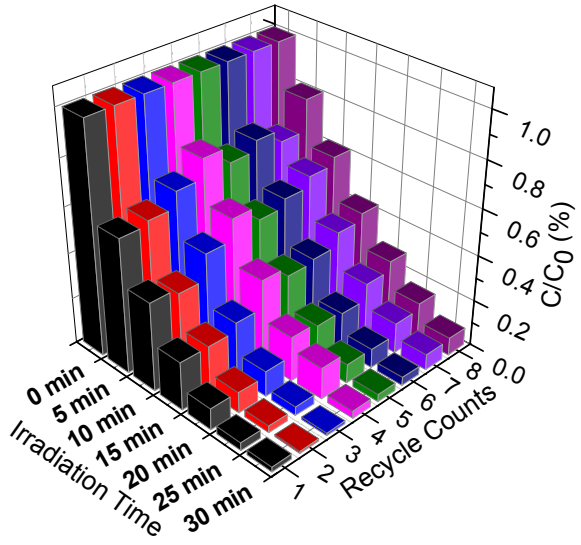

Fig. 7 Cycling runs for the photocatalytic MO degradation in the presence of Ag@AgCl (A-30) nanoframe photocatalysts.

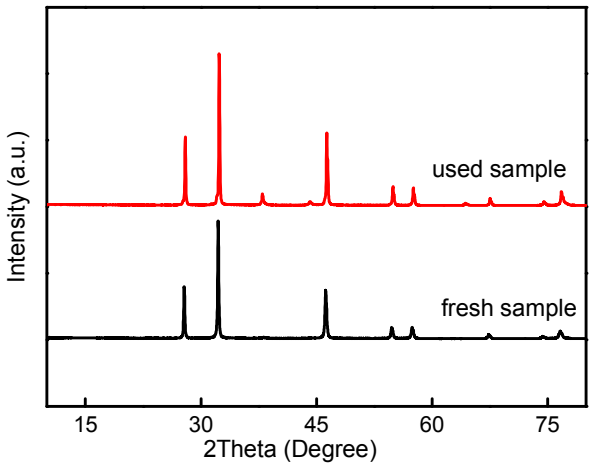

Fig. 8 XRD patterns of the Ag@AgCl (A-30) nanoframes after 8 runs cycling photocatalytic experiment.

It is generally accepted that organic pollutants can be degraded by photocatalytic oxidation processes, in which a series of photo-induced reactive species, such as h^+, •OH, and $•O_2^-$, are suspected to be involved in the photocatalytic degradation reaction. To elucidate the main reactive species responsible for the degradation of organic contaminants over Ag@AgCl photocatalyst under visible-light irradiation, the ESR spin-trap technique with 5, 5-dimethyl-1-pyrroline N-oxide (DMPO) is used to detect radicals in reaction systems. DMPO is a nitrone spin trap generally used for trapping radicals: DMPO-•OH or DMPO-$•O_2^-$. As shown in Fig.9, there is no ESR signal in the dark. A gradual evolution of ESR peaks for DMPO-$•O_2^-$ adducts in H_2O and DMSO was observed with visible light irradiation, which is in accordance with the previous literature. [39-41] In contrast, no signals of DMPO-•OH adducts were detected in H_2O and DMSO. Dong et al.[30] demonstrated a similar ESR result that superoxide radical was produced by the photo-activated Ag@AgCl under visible light irradiation. The ESR results confirm that $•O_2^-$ radicals exist in the Ag@AgCl nanoframes system under visible light irradiation.

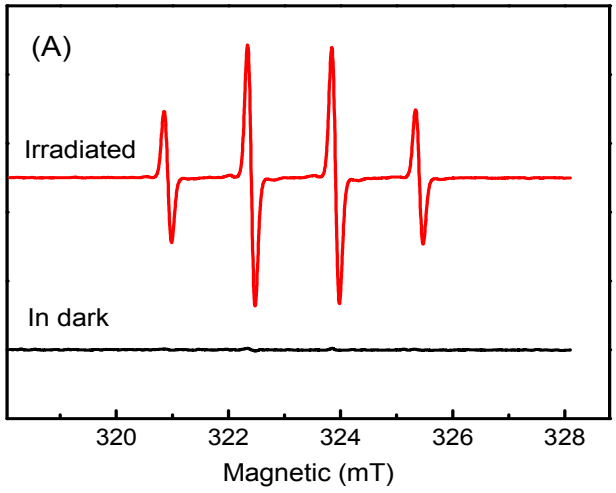

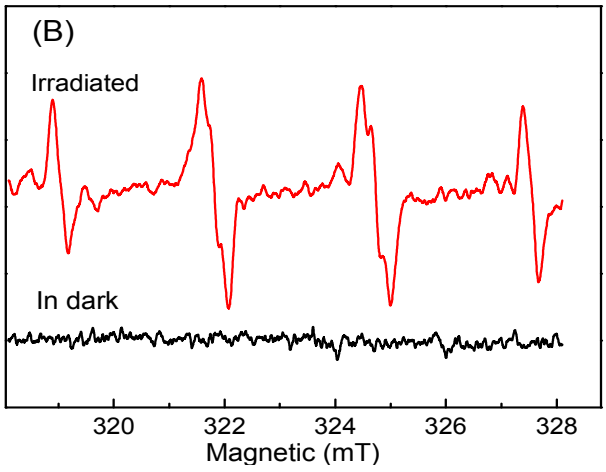

Fig. 9 ESR spectra recorded at ambient temperature with Ag@AgCl (A-30) nanoframe photocatalyst in: (A) H_2O (B) DMPO

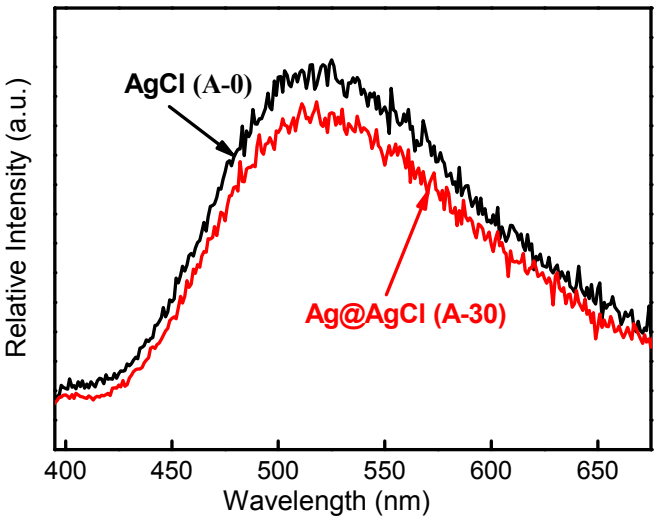

Fig.10 Photoluminescence spectra (PL) of the AgCl (A-0) and Ag@AgCl (A-30) photocatalysts.

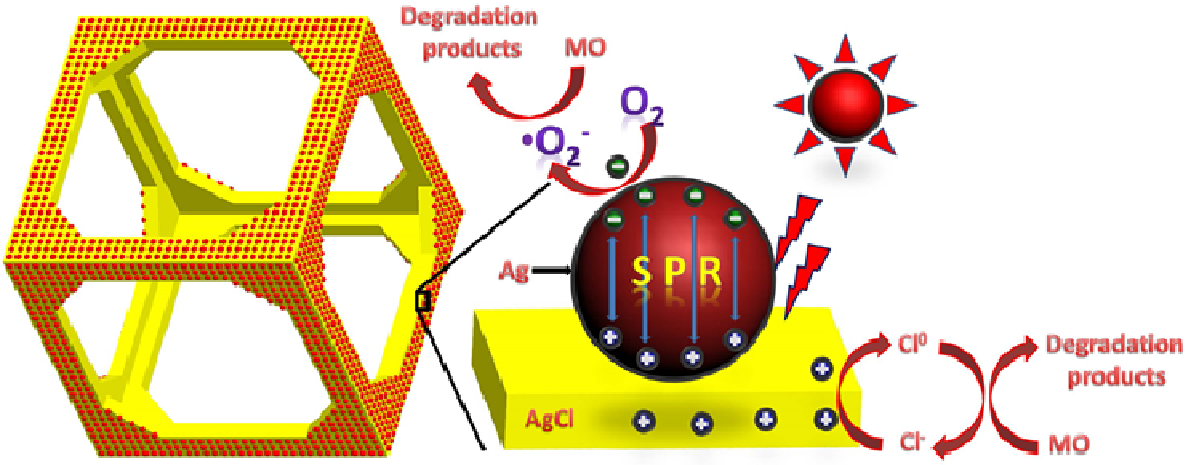

Fig.12 Schematic diagram illustrating the production of Ag NPs on AgCl and the proposed degradation mechanism of organic pollutants over Ag@AgCl plasmonic nanoframes.

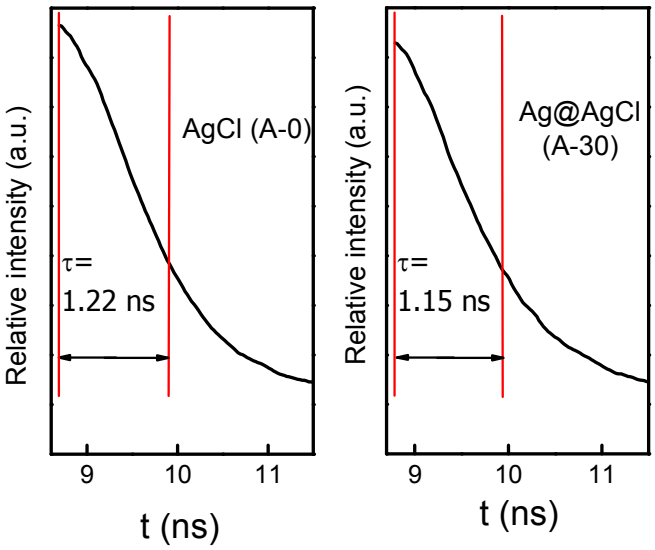

Fig.11 The transient photoluminescence spectra of AgCl (A-0) and Ag@AgCl (A-30) nanoframe samples.

Combined with ESR results in Fig.9, superoxide radical are still the main oxidative species for Ag@AgCl samples. Therefore, the efficient photocatalytic degradation of MO can smoothly proceed. To further investigate the effect of Ag NPs modification, the PL spectra of Ag@AgCl were performed. PL spectra reveal the migration, transfer, and recombination processes of the photogenerated electron-hole pairs in semiconductors. Fig.10 presents the PL spectra of the Ag@AgCl nanoframe (A-30) and pure AgCl (A-0) photocatalysts at an excitation wavelength of 395nm. At room temperature, the emission band for pure AgCl was centered at 525nm, which was attributed to the recombination process of self-trapped excitations. The positions of the Ag@AgCl emission peaks were similar to AgCl. However, the emission intensity of Ag@AgCl photocatalyts decreased. To further investigate the mechanism, the photoluminescence life time measurement was also performed (Fig.11). The luminescence lifetime of the A-30 and A-0 photocatalysts was determined to be 1.15 and 1.22 ns, respectively. The short PL life time indicated that the charge carriers in Ag@AgCl nanoframe (A-30 sample) have high migration and separation efficiency. Therefore, the PL results clearly indicated that recombination of photo-generated electron-hole pairs in Ag@AgCl nanoframe was effectively restrained.

The degradation mechanism of organic pollutants over Ag@AgCl plasmonic photoctalyst is schematically illustrated in Fig.12. The localized surface plasmon state of a silver nanoparticle lies in the visible light region; therefore the absorption of visible light by the Ag@AgCl catalyst takes places at the silver surfaces. Due to the SPR effect, photogenerated electron-hole pairs are formed on the surface of Ag NPs under visible irradiation. Subsequently, the electrons will be trapped by absorbed O_2 to form $\bullet O_2^-$. Holes transfer to the AgCl surface corresponds to the oxidation of Cl^- ions to Cl^0 atoms. Both $\bullet O_2^-$ and Cl^0 are reactive active species responsible for the degradation of organic pollutants. As Cl^0 are reactive radical species, they should be able to oxidize MO dye and hence are reduced to Cl^- again. As a result, the Ag@AgCl plasmonic nanoframes exhibit superior activity for decomposition of organic pollutants.

4. Conclusions

In this work, we successfully synthesized the plasmonic photocatalyst Ag@AgCl with nanoframe morpholgy via a simple site-selected synthesis and light-induced chemical process. The strong SPR effect of Ag NPs on the surface can generate electron-hole pairs and the synergistic effects effectively promote interfacial charge transfer, leading to the enhancement of the photocatalytic activities of Ag@AgCl samples. ESR tests with DMPO confirmed that $\bullet O_2^-$ and Cl^0 are likely to be the reactive species responsible for the degradation of organics. More importantly, the sited-section synthesis process opens up a new possibility to fabricate other similar functional materials.

[a] Key Laboratory of Heavy Oil Processing, College of Science, China University of Petroleum Beijing, No. 18 Fuxue Rd., Beijing 102249, People's Republic of China.

[b] Department of Materials Science and Engineering, College of Science, China University of Petroleum Beijing, No. 18 Fuxue Rd., Beijing 102249, People's Republic of China.
Corresponding Author：*E-mail: gelei08@sina.com (Professor Lei Ge)，**Tel:** +86-10-89739096
Electronic Supplementary Information (ESI) available: [details of any supplementary information available should be included here]. See DOI: 10.1039/b000000x/

Acknowledgements

This work was financially supported by the National Science Foundation of China (Grant No. 21003157 and 21273285), Beijing Nova Program (Grant No. 2008B76), and Science Foundation of China University of Petroleum, Beijing (Grant No. KYJJ2012-06-20).

Notes and references

1 A. Fujishima and K. Honda, *Nature*, 1972, **238,** 37-38.
2 G. Liu, Y. Zhao, C. Sun, F. Li, G. Q. Lu and H. M. Cheng, *Angew. Chem., Int. Ed.*, 2008, **47,** 4516-4520.
3 X. Chen, H. Y. Zhu, J. C. Zhao, Z. F. Zheng and X. P. Gao, *Angew. Chem.*, 2008, **120**, 5433-5436.
4 A. Kudo and Y. Miseki, *Chem. Soc. Rev.*, 2009, **38**, 253-278.
5 Y. G. Sun and Y. N. Xia, *Science*, 2002, **298,** 2176-2179.
6 G. Wang, B. B. Hang, X. C. Ma, Z. Y. Wang, X. Y. Qin, X. Y. Zhang,Y. Dai and M. H. Whangbo, *Angew. Chem.*, 2013,**52**,4810-4813.
7 X. B. Chen and S. S. Mao, *Chem. Rev.*, 2007, **107**, 2891-2959.
8 P. Xu, T. Xu, J. Lu, S. M. Gao, N. S. Hosmane, B. B. Huang, Y. Dai and Y. B. Wang, *Energy Environ. Sci.*, 2010, **3**, 1128-1134.
9 J. G. Yu, G. P. Dai and B. B. Huang, *J. Phys. Chem. C*, 2009, **113**, 16394-16401.
10 Z. K. Zheng, B. B. Huang, X. D. Meng, J. P. Wang, Z. Z. Lou, Z. Y. Wang, X. Y. Qin, X. Y. Zhang and Y. Dai, *Chem. Commun.*, 2013, **49**, 868-870.
11 O. S. David, W. D. Charles, B. John, A. S. Stephen, J. L. Andrew, M. W. Scott, A. C. Richard, J. P. Michael, G. P. Robert, P. P. Lvan, W. W. Graeme, W. K. Thomas, S. Paul, W. Aron and A. S. Alexey, *Nat. Mater.*, 2013, **12**, 798-801.
12 Z. Hosseini, N. Taghavinia, N. Sharifi, M. Chavoshi and M. Rahman, *J. Phys. Chem. C*, 2008, **112,** 18686-18689.
13 U. M. K. Shahed, A. S. Mofareh, B. William and J. Ingler, *Science*, 2002, **297**, 2243-2245.
14 W. P. Qin, D. S. Zhang, D. Zhao, L. L. Wang and K. Z. Zheng, *Chem. Commun.*, 2010, **46**, 2304-2306.
15 P. Wang, B. B. Huang, Y. Dai and M. H. Whangbo, *Phys. Chem. Chem. Phys.*, 2012, **14**, 9813-9825.
16 J. Tian, Y. H. Sang, G. W. Yu, H. D. Jiang, X. N. Mu and H. Liu, *Adv. Mater.*, 2013, **25,** 5075-5080.
17 Z. K. Zheng, B. B. Huang, X. Y. Qin, X. Y. Zhang, Y. Dai and M. H. Whangbo, *J. Mater. Chem.*, 2011, **21,** 9079-9087.
18 P. Wang, B. B. Huang, X. Y. Zhang, X. Y. Qin, H. Jin, Y. Dai, Z. Y. Wang, J. Y. Wei, J. Zhan, S. Y. Wang, J. P. Wang and M. H. Whangbo, *Chem. Eur. J.*, 2009,**15**, 1821-1824.
19 L. Ge, C. C. Han, J. Liu, Y. F. Li, *Appl. Catal., A*, 2011, **409-410**, 215-222.
20 X. J. Bai, R. L. Zong, C. X. Li, D. Liu, Y. F. Liu and Y. F. Zhu, *Appl. Catal., B*, 2014, **147,** 82-91.
21 H. Zhang, X. F. Fan, X. Quan, S. Chen and H. T. Yu, *Environ. Sci. Technol.*, 2011, **45,** 5731-5736.
22 P. Wang, B. B. Huang, X. Y. Qin, X. Y. Zhang, Y. Dai, J. Y. Wei and M. H. Whangbo, *Angew. Chem. Int. Ed.*, 2008, **47**, 7931-7933.
23 P. Wang, B. B. Huang, X. Y. Zhang, X. Y. Qin, Y. Dai, Z. Y. Wang and Z. Z. Lou, *ChemCatChem.*,2011, **3**, 360-364.
24 Y. P. Bai, S. X. Ouyang, N. Umezawa, Z. Y. Cao and J. H. Ye, *J. Am. Chem. Soc.*, 2011,**133,** 6490-6492.
25 H. C. Zhang, H. Huang, H. Ming, H. T. Li, L. L. Zhang, Y. Liu and Z. H. Kang, *J. Mater. Chem.*, 2012, **22**, 10501-10506.
26 G. P. Dai, J. G. Yu and G. Liu, *J. Phys. Chem. C*, 2012, **116,** 15519-15524.
27 C. Dong, K. L. Wu, X. W. Wei, X. Z. Li, L. Liu, T. H. Ding, J. Wang and Y. Ye, *CrystEngComm.*, 2014, **16**, 730-736.
28 C. H. An, S. Peng and Y. G. Sun, *Adv. Mater.*, 2010, **22**, 2570-2574.
29 Y. X. Tang, Z. L. Jiang, G. H. Xing, A. R. Li, P. D. Kanhere, Y. Y. Zhang, T. C. Sum, S. Z. Li, X. D. Chen, Z. L. Dong and Z. Chen, *Adv. Funct. Mater.*, 2013, **23**, 2932-2940.
30 R. F. Dong, B. Z. Tian, C. Y. Zeng, T. Y. Li, T. T. Wang, J. L. Zhong, *J. Phys. Chem. C*, 2013, **117,** 213-220.
31 X. H. Xia, Y. Wang, A. Ruditskiy and Y. N. Xia, *Adv. Mater.*, 2013, **25,** 6313-6333.
32 J. W. Nai, Y. Tian, X. Guan and L. Guo, *J. Am. Chem. Soc.*, 2013, **135,** 16082-16091.
33 V. G. Plotnichenko, D. V. Philippovskiy, V. O. Sokolov, V. F. Golovanov, G. V. Polyakova, L. S. Lisitsky and E. M. Dianov, *Optics Letters*, 2013, **38,** 2965-2968.
34 Y. G. Sun, *nanoscale*, 2010, **2**, 1626-1642.
35 Y. Wang, Y. Q. Zheng, C. Z. Huang and Y. N. Xia, *J. Am. Chem. Soc.*, 2013,**135**, 1941-1951.
36 D. Chen, T. Li, Q. Q. Chen, J. B. Gao, B. B. Fan, J. Li, X. J. Li, R. Zhang, J. Sun and L. Gao, *Nanoscale*, 2012, **4**, 5431-5439.
37 M. Zhu, P. Chen and M. Liu, *ACS Nano*, 2011, **5**, 4529-4536.
38 M. Zhu, P. Chen and M. Liu, *Langmuir*, 2012, **28**, 3385-3390.
39 X. F. Zhou, C. Hu, X. X. Hu, T. W. Peng and J. H. Qu, *J. Phys. Chem. C*, 2010,**11**,2746-2750.
40 X. J. Bai, L. Wang, R. L. Zong and Y. F. Zhu, *J. Phys. Chem. C*, 2013, **117**, 9952-9961.
41 C. C. Han, L. Ge, C. F. Chen, Y. J. Li, X. L. Xiao, Y. N. Zhang, L. L. Guo, *Appl. Catal., B*, 2014, **147**, 546-553.

Graphical Abstract

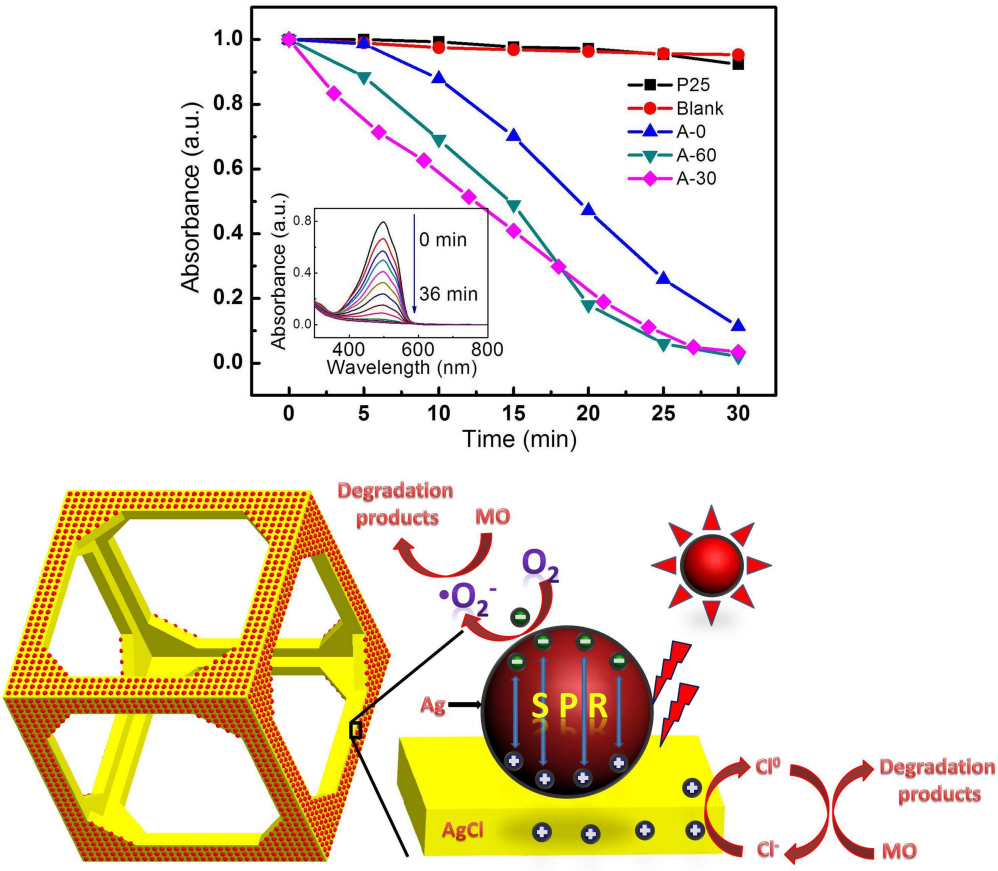

The novel Ag@AgCl nanoframes with efficient visible-light-induced photocatalytic activity are developed via a site-selected growth process, and Ag nanoparticles play a key role in the photocatalysts.